STRESS-CRACK OPENING RELATIONSHIP OF ENHANCED PERFORMANCE CONCRETE

J.M. Sena Cruz[*], J.A.O. Barros[*], A.R. Fernandes[*], A.F.M. Azevedo[**], A. Camões[*]

***Department of Civil Engineering**
Universidade do Minho
Azurém, 4800-058 Guimarães
****Department of Civil Engineering**
Faculdade de Engenharia da Universidade do Porto
Rua Dr. Roberto Frias, S/N, 4200-465 Porto

Abstract. Force-deflection responses obtained from three-point bending tests with notched beams of enhanced performance concrete were used to determine, by means of an inverse analysis, the stress at crack initiation, the shape of the stress-crack opening relationship and the fracture energy of this material. This inverse analysis was performed with non-linear finite element software where crack opening and crack propagation were simulated by discrete crack models using interface finite elements. The influence of both the concrete age and the percentage of binder replaced by fly-ash on the fracture parameters was analysed. In the present work, the numerical strategy is described, and the obtained results are presented and analysed.

1. INTRODUCTION

Crack formation and crack propagation are the mandatory phenomena responsible for the non-linear behaviour of concrete structures. Therefore, to evaluate the deformational response of a concrete structure up to its collapse load, the concrete post-cracking behaviour should be assessed as accurately as possible. To characterize the concrete post-cracking behaviour, RILEM [1] proposed a bending test, from which the flexural tensile strength, the fracture energy and the shape of the stress-crack opening relationship can be derived. These concrete fracture parameters can be used to define the fracture mode I of a constitutive law of an interface element that is currently used in the modelling of geometrical discontinuities in several structural engineer problems [2-5]. Crack propagation can also be assumed as a geometrical discontinuity, since a discontinuity in the displacement field occurs when a crack is formed. Accurate stress distribution around the crack can only be assured if crack propagation is simulated by interface elements using a discrete modelling approach [6].

In the last decades, efforts were made to increase the strength [7] of cement-based materials. Compression above 600 MPa was already attained but, when compared with conventional concrete, the amount of binder that this ultra-high performance concrete requires is much larger [7]. Due to economical and environmental consciousness, the improvements in concrete performance should be attained with the use of relatively low cost binder materials [8], such as fly ash (*Fa*). To characterize the post-cracking behaviour of enhanced performance concrete several series of bending tests were carried out according to the RILEM recommendations. The influence of both the percentage of binder replaced by *Fa* and the age of the concrete specimen was analysed. Using an inverse analysis and the force-deflection relationships recorded from these tests, the values of the concrete fracture parameters were obtained. In the present work, the numerical strategy applied is described and the main results are presented and analysed.

2. FORMULATION OF THE 2D LINE INTERFACE FINITE ELEMENT

The six-node 2D line interface finite element used in the present analysis is schematically represented in Fig. 1. This element was implemented in the computational code named FEMIX [9]. In Fig. 1 x_i' is the 2D line interface finite elements local coordinate system, where x_1' is the tangent axis and x_2' the normal axis. In x_i', the continuous displacement field is

$$\underline{u}' = \begin{bmatrix} u'_{B1} & u'_{B2} & u'_{T1} & u'_{T2} \end{bmatrix}^T \qquad (1)$$

where u'_{Bi} and u'_{Ti} is the displacement in the i^{th} direction at bottom and top sides of the 2D line

interface finite elements, respectively. The element nodal displacements in x_i' coordinate system are grouped in the vector $\underline{a}'$

$$\underline{a}' = [a'_{11} \quad a'_{12} \mid a'_{21} \quad a'_{22} \mid a'_{31} \quad a'_{32} \mid \ldots \\ \ldots \mid a'_{41} \quad a'_{42} \mid a'_{51} \quad a'_{52} \mid a'_{61} \quad a'_{62}]^T \tag{2}$$

where a'_{ij} is the displacement of node *i* in the x'_j direction.

The continuous displacement field is obtained from the element nodal displacements using the interpolation

$$\underline{u}' = \underline{N}\,\underline{a}' \tag{3}$$

where $\underline{N}$ is the matrix of the shape functions.

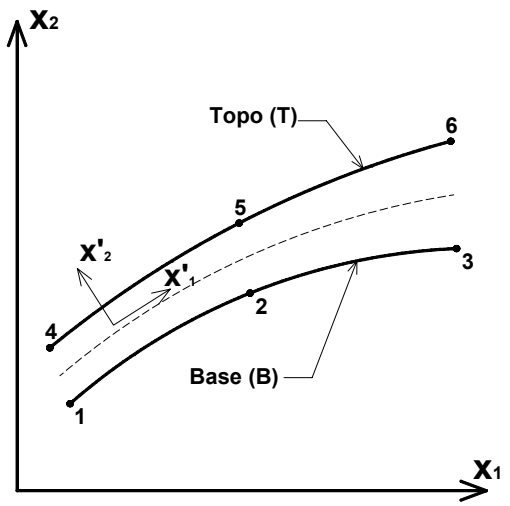

Fig. 1 - Quadratic line interface finite element

Equation (3) in expanded format reads

$$\begin{bmatrix} u'_{B1} \\ u'_{B2} \\ u'_{T1} \\ u'_{T2} \end{bmatrix} = \left[\begin{array}{cc|cc|cc|cc|cc|cc} N_1 & 0 & N_2 & 0 & N_3 & 0 & 0 & 0 & 0 & 0 & 0 & 0 \\ 0 & N_1 & 0 & N_2 & 0 & N_3 & 0 & 0 & 0 & 0 & 0 & 0 \\ 0 & 0 & 0 & 0 & 0 & 0 & N_4 & 0 & N_5 & 0 & N_6 & 0 \\ 0 & 0 & 0 & 0 & 0 & 0 & 0 & N_4 & 0 & N_5 & 0 & N_6 \end{array}\right] \begin{bmatrix} a'_{11} \\ a'_{12} \\ a'_{21} \\ a'_{22} \\ a'_{31} \\ a'_{32} \\ a'_{41} \\ a'_{42} \\ a'_{51} \\ a'_{52} \\ a'_{61} \\ a'_{62} \end{bmatrix} \tag{4}$$

where N_i is the i^{th} shape function of a three-node linear element [10]. The components of the relative displacement vector, $\Delta\underline{u}'$, represent the crack sliding, *s*, and the crack opening, *w*. These components can be obtained from the $\underline{u}'$ vector:

$$\begin{aligned} \Delta\underline{u}' &= \begin{bmatrix} s \\ w \end{bmatrix} = \begin{bmatrix} \Delta u'_1 \\ \Delta u'_2 \end{bmatrix} = \begin{bmatrix} u'_{T1} - u'_{B1} \\ u'_{T2} - u'_{B2} \end{bmatrix} \\ &= \begin{bmatrix} -1 & 0 & 1 & 0 \\ 0 & -1 & 0 & 1 \end{bmatrix} \begin{bmatrix} u'_{B1} \\ u'_{B2} \\ u'_{T1} \\ u'_{T2} \end{bmatrix} \\ &= \underline{L}\,\underline{u}' \end{aligned} \tag{5}$$

Substituting (3) into (5) results:

$$\begin{aligned} \Delta\underline{u}' &= \underline{L}\,\underline{N}\,\underline{a}' \\ &= \underline{B}\,\underline{a}' \end{aligned} \tag{6}$$

where

$$\underline{B} = \underline{L}\,\underline{N} \tag{7}$$

is the relative displacement-nodal displacement matrix:

$$\underline{B} = \begin{bmatrix} -1 & 0 & 1 & 0 \\ 0 & -1 & 0 & 1 \end{bmatrix} \left[\begin{array}{cc|cc|cc|cc|cc|cc} N_1 & 0 & N_2 & 0 & N_3 & 0 & 0 & 0 & 0 & 0 & 0 & 0 \\ 0 & N_1 & 0 & N_2 & 0 & N_3 & 0 & 0 & 0 & 0 & 0 & 0 \\ 0 & 0 & 0 & 0 & 0 & 0 & N_4 & 0 & N_5 & 0 & N_6 & 0 \\ 0 & 0 & 0 & 0 & 0 & 0 & 0 & N_4 & 0 & N_5 & 0 & N_6 \end{array}\right]$$
$$= \left[\begin{array}{cc|cc|cc|cc|cc|cc} -N_1 & 0 & -N_2 & 0 & -N_3 & 0 & N_4 & 0 & N_5 & 0 & N_6 & 0 \\ 0 & -N_1 & 0 & -N_2 & 0 & -N_3 & 0 & N_4 & 0 & N_5 & 0 & N_6 \end{array}\right] \quad (8)$$

The constitutive behaviour of the interface element is simulated with the following traction-relative displacement relationship:

$$\underline{\sigma}' = \begin{bmatrix} \tau \\ \sigma \end{bmatrix} = \begin{bmatrix} \sigma_1' \\ \sigma_2' \end{bmatrix} = \underline{D}\,\Delta\underline{u}' \quad (9)$$

where $\underline{\sigma}'$ is a vector, whose components are the tangential ($\tau = \sigma_1'$) and normal ($\sigma = \sigma_2'$) stress, and $\underline{D}$ is the constitutive matrix

$$\underline{D} = \begin{bmatrix} D_t & 0 \\ 0 & D_n \end{bmatrix} \quad (10)$$

with D_t and D_n being the tangential and normal stiffness. For accurate simulations of structural problems governed by crack propagation, appropriate laws defining D_t and D_n should be used.

From the principle of virtual work (PVW), the internal work is:

$$W_{\text{int}} = \int_S \delta\left(\Delta\underline{u}'\right)^T \underline{\sigma}'\, dS \quad (11)$$

where $\delta\left(\Delta\underline{u}'\right)^T$ is the virtual relative displacement vector. The element nodal displacement vector in the local coordinate system, $\underline{a}'$, can be obtained from the element nodal displacement vector in the global coordinate system, $\underline{a}'$:

$$\underline{a}' = \underline{T}\,\underline{a} \quad (12)$$

where $\underline{T}$ is the transformation matrix. Replacing (12) into (6):

$$\Delta\underline{u}' = \underline{B}\,\underline{a}' = \underline{B}\,\underline{T}\,\underline{a} \quad (13)$$

and (13) into (9)

$$\underline{\sigma}' = \underline{D}\,\underline{B}\,\underline{T}\,\underline{a} \quad (14)$$

Substituting (13) and (14) into (11) yields,

$$W_{\text{int}} = \int_S \delta\underline{a}^T\, \underline{T}^T\, \underline{B}^T\, \underline{D}\,\underline{B}\,\underline{T}\,\underline{a}\, dS$$
$$= \delta\underline{a}^T \int_S \underline{T}^T \underline{B}^T\, \underline{D}\,\underline{B}\,\underline{T}\, dS\, \underline{a} \quad (15)$$

The work produced by the external forces due to virtual displacements is given by

$$W_{ext} = \delta\left(\underline{a}'\right)^T\, \underline{F}' \quad (16)$$

where

$$\underline{F}' = \underline{T}\,\underline{F} \quad (17)$$

Substituting (12) and (17) into (16) yields

$$W_{ext} = \delta\underline{a}^T\, \underline{T}^T\, \underline{T}\,\underline{F}$$
$$= \delta\underline{a}^T\, \underline{F} \quad (18)$$

From the PVW ($W_{ext} = W_{\text{int}}$),

$$\int_S \underline{T}^T\, \underline{B}^T\, \underline{D}\,\underline{B}\,\underline{T}\, dS\, \underline{a} = \underline{F} \quad (19)$$

or

$$\underline{K}\,\underline{a} = \underline{F} \quad (20)$$

where

$$\underline{K} = \int_S \underline{T}^T\, \underline{B}^T\, \underline{D}\,\underline{B}\,\underline{T}\, dS \quad (21)$$

is the element stiffness matrix and $\underline{F}$ is the element external load vector.

In the incremental and iterative procedure of a non-linear analysis problem, the external load vector is the current residual load vector, which is the difference between the applied external load vector and the internal equivalent forces. This last one is evaluated with the following expression:

$$\underline{F}'_{\text{int}} = \int_S \left(\Delta \underline{u}'\right)^T \underline{\sigma}'\, dS = \int_S \left(\underline{a}'\right)^T \underline{B}^T \underline{\sigma}'\, dS = \int_S \left(\underline{a}'\right)^T \underline{T}^T \underline{B}^T \underline{\sigma}'\, dS \tag{22}$$

where $\underline{\sigma}'$ is calculated in each integration point of the interface element, using equation (9). In the present work the bi-linear diagram represented in Fig. 2 is used to evaluate the normal stiffness, k_n, since previous works have shown that this diagram is suitable to model the post-cracking behaviour of plain concrete [6, 11]. The fracture energy, G_f, is the area under the $\sigma - w$ diagram.

3. APPRAISAL OF THE NUMERICAL MODEL

To assess the model performance, the force-deflection relationship obtained with a widely used computational code in the simulation of a three point bending test with an un-notched steel fibre reinforced concrete beam was used for comparison purposes [12]. The cross section of the specimen is 150×150 mm^2 and its span is 500 mm. 2D line interface finite elements were located in the specimen's symmetry axis. In the remaining parts of the specimen linear eight-node Serendipity plane-stress elements were used.

Gauss-Lobatto integration scheme [5] with three integration points (IP) was used for the 2D line interface finite elements, while Gauss-Legendre integration scheme with 2×2 IP was used for the eight-node elements. According to the available data [12], the values of the Young's modulus, Poisson coefficient, σ_1, w_2, σ_2 and w_3 are 35000 N/mm^2, 0.2, 3.0 N/mm^2, 0.05 mm, 1.491 N/mm^2 and 10 mm, respectively. To avoid undesired spurious oscillations of the stress field a value of 1.0×10^4 N/mm^3 was assigned to the initial D_n stiffness [5]. Since in this problem sliding does not occur in the interface elements, the analysis is independent of the values assigned to D_t.

The force-deflection curve obtained with the developed model (FEMIX) is practically coincident with the curve determined using the DIANA computational package.

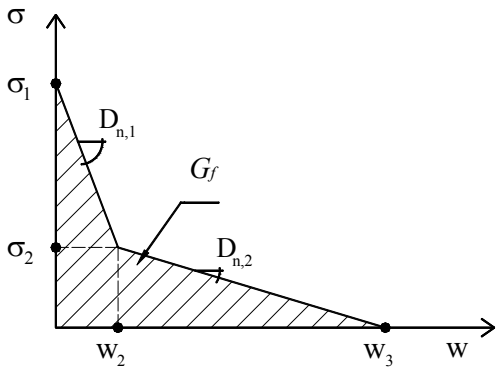

Fig. 2 - Stress-crack opening diagram

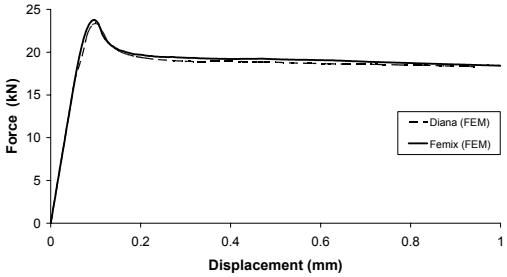

Fig. 3 - Force-deflection relationship obtained with DIANA and FEMIX computational codes

4. ASSESSING THE FRACTURE PARAMETERS

4.1. Numerical strategy

To assess the concrete fracture parameters an inverse analysis was performed, evaluating the values of the σ_i and w_i of the $\sigma - w$ diagram that fit the experimental $F - \delta$ curves with the minimum error of the parameter

$$err = \left| A^{\text{exp}}_{F-\delta} - A^{num}_{F-\delta} \right| \Big/ A^{\text{exp}}_{F-\delta} \tag{23}$$

where $A^{\text{exp}}_{F-\delta}$ and $A^{num}_{F-\delta}$ are the areas below the experimental and the numerical $F - \delta$ curve, respectively. Fig. 4 shows the finite element mesh used. The type of elements and the integration rules adopted in this section were coincident with the ones used in the previous section. Since a large scatter was obtained in the concrete Young's Modulus, E_c, from the uniaxial compression tests [13] the value of E_c considered in each numerical analysis was the one that has best fit the experimental $F - \delta$ curve up to crack initiation.

The adequacy of the numerical strategy adopted is shown in Fig. 5, revealing that the proposed bilinear $\sigma - w$ diagram is capable of predicting, with enough accuracy, the post-cracking behaviour of the tested

specimens. The experimental $F-\delta$ curve is the average of the responses obtained from three specimens. The concrete of the series of Fig. 5 had a composition of 500 kg/m^3 of binder (cement plus fly-ash, B500), 0% and 60% of the binder replaced by fly ash (Fa0, Fa60), and the curing period of time was 28 days (Ag28). The specimens were tested at the end of the curing period of time. Similar performances were obtained in the remaining series of tests.

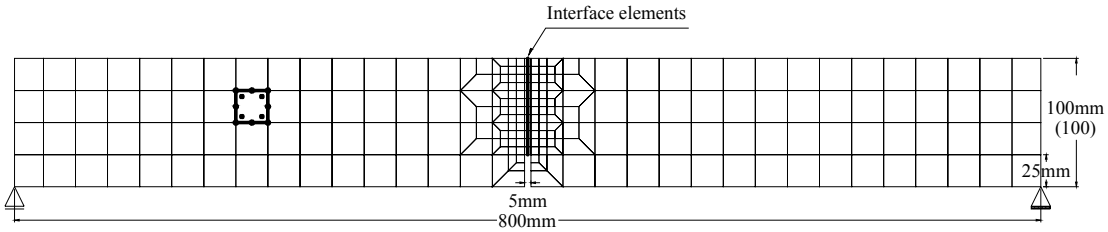

Fig. 4 - Finite element mesh adopted in the numerical simulation

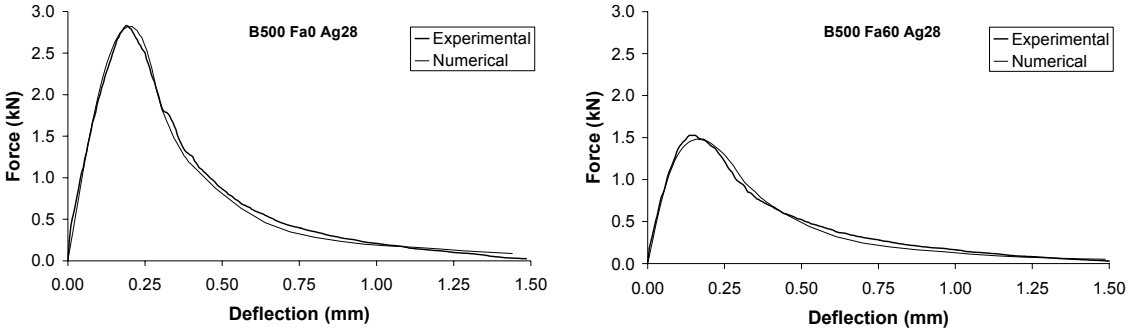

Fig. 5 - Comparison between experimental and numerical $F-\delta$ curves

Using the $\sigma-w$ diagram recommended by CEB-FIP Model Code [14], a lower residual force is predicted after peak load and the deflection at peak load is smaller than the deflection recorded in the experimental tests, see Fig. 6. The peak load is, however, correctly predicted. In this figure the $F-\delta$ relationship obtained with the FEMIX software was also included. The $\sigma-w$ diagram of CEB-FIP and the $\sigma-w$ diagram obtained from inverse analysis with FEMIX are depicted in Fig. 7. When compared to the CEB-FIP $\sigma-w$ diagram, the one obtained from inverse analysis has lower values of σ_1 and $D_{n,1}$, and similar values of σ_2. This tendency was observed in the simulations of the remaining series.

4.2. Fracture parameters

Based on the bilinear $\sigma-w$ diagram, with which the experimental force-deflection curves were best fit, the corresponding fracture energy values ($G_{f,NUM}$) were obtained and compared with the experimental ones ($G_{f,EXP}$), see Fig. 8. The experimental fracture energy values result from the addition of the work due to the load applied by the actuator with the work resulting from the contribution of the specimen self-weight [1, 11]. The influence of the self-weight was also included in $G_{f,NUM}$. The values of $G_{f,NUM}$ were 8% larger than $G_{f,EXP}$ since with a bilinear $\sigma-w$ diagram a $F-\delta$ longer tail was predicted by the numerical analysis. To fit more accurately the end part of the experimental $F-\delta$ curve, a trilinear $\sigma-w$ diagram should be used [15].

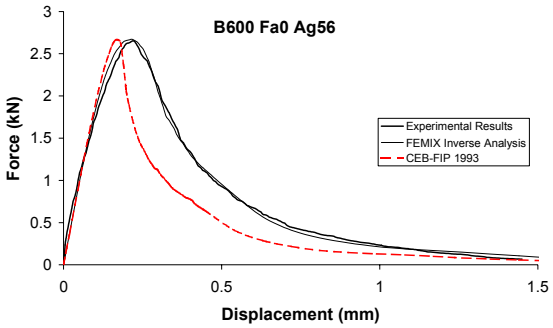

Fig. 6 - Force-deflection curves using the $\sigma - w$ diagram of CEB-FIP 1993 and the inverse analysis with FEMIX

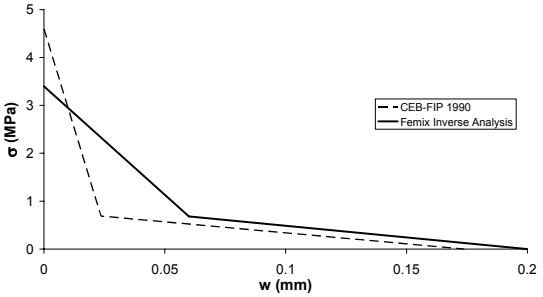

Fig. 7 - Stress-crack opening softening diagram of CEB-FIP [15] and from inverse analysis

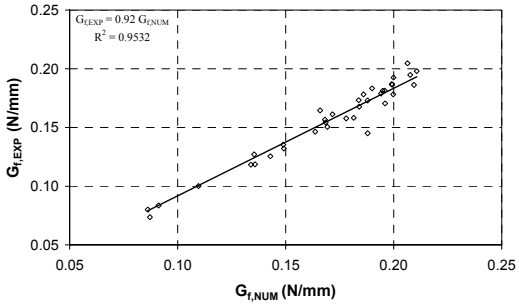

Fig. 8 - Relationship between the fracture energy obtained from numerical and experimental approaches

Figs. 9 to 13 show the influence of the age of the concrete specimens when tested (Ag) and the percentage of binder replaced by fly ash on the parameters defining the concrete post-cracking behaviour (see Fig. 2). Each figure is composed by two graphs, one for the compositions with 500 kg/m^3 of binder (B500) and the other for the compositions with B=600 kg/m^3. According to the results obtained, G_f increases with the specimen's age, but this increase is marginal after 156 days. Furthermore, G_f decreases with the increase of the percentage of binder replaced by *Fa*, mainly at specimens of young age. Increasing the specimen's age, the influence of this replacement on G_f is attenuated, becoming marginal for a replacement of 20%.

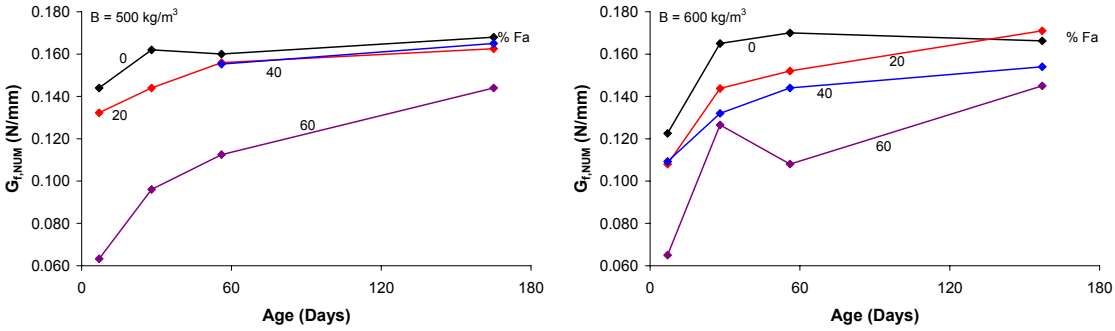

Fig. 9 - Influence of both the specimen's age and the percentage of binder replaced by *Fa* on $G_{f,NUM}$

Figs. 10 and 11 show that, in general, σ_1 and σ_2 increase with the age up to a maximum that occurred between 30 and 60 days. After 60 days, σ_1 and σ_2 are not significantly influenced by the concrete age. In most cases, increasing the percentage of binder replaced by *Fa* results in a decrease of the values of σ_1 and σ_2.

Fig. 12 shows that, except for series of Fa0 and Fa20 with B=600 kg/m^3, in the remaining series $D_{n,1}$ has increased with the age up to a maximum that occurred between 30 and 60 days. After this age, the major part of the series shows a decreasing tendency of $D_{n,1}$ with the age, revealing a raise in the pseudo-ductility of the concrete with its age, i.e., a higher stress retention just after crack initiation. The

maximum $D_{n,1}$ appears to be attained at older ages as large is the content of binder. In general, increasing the percentage of *Fa* causes a decrease of $D_{n,1}$.

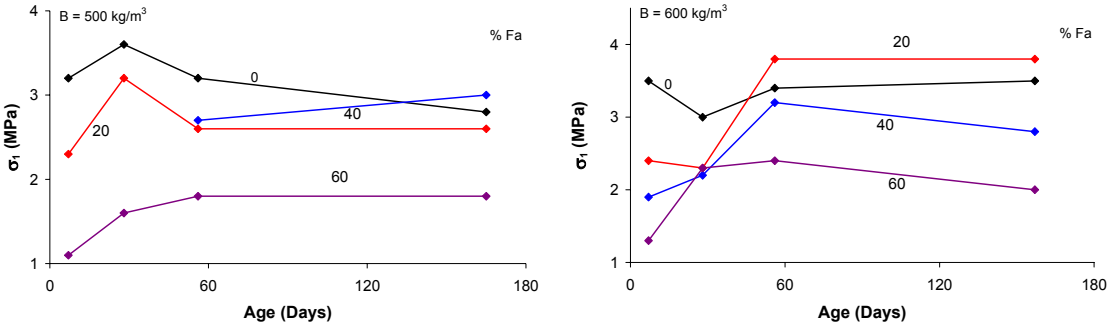

Fig. 10 - Influence of both the specimen's age and the percentage of binder replaced by *Fa* on σ_1

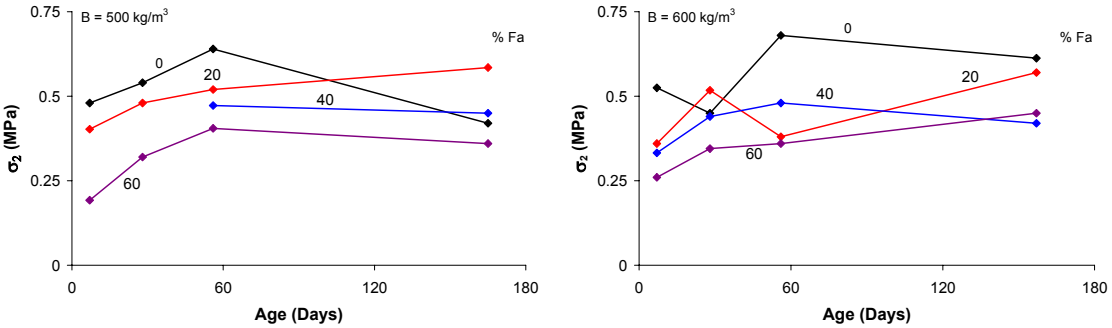

Fig. 11 - Influence of both the specimen's age and the percentage of binder replaced by *Fa* on σ_2

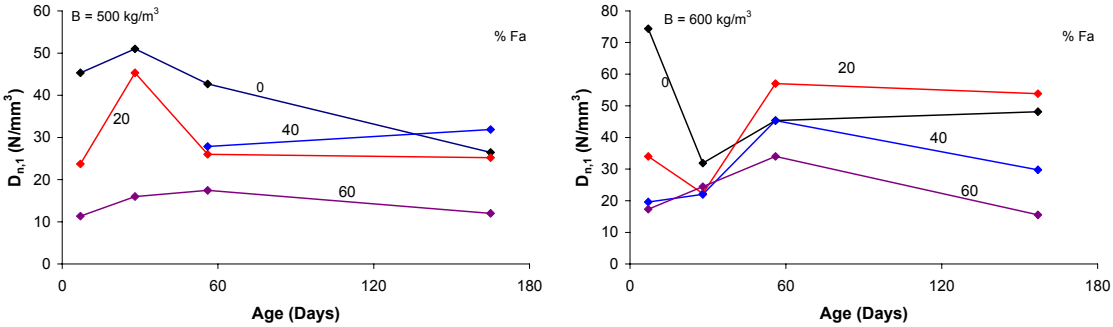

Fig. 12 - Influences of the specimen's age at testing and the percentage of binder replaced by *Fa* on the $D_{n,1}$

Fig. 13 reveals that there is an increase tendency of $D_{n,2}$ with the specimen's age. In some series the maximum value of $D_{n,2}$ seems to be not attained, even for a testing age of about 156 days. This is more emphasised in the series where some percentage of the binder was replaced by *Fa*.

Using the compression strength values obtained experimentally, the corresponding average tensile strength, f_{ctm}, was evaluated from the recommendations of CEB-FIP 1990 Model Code [14]. Fig. 14 shows the relationships $\sigma_1 - f_{ctm}$ and $\sigma_2 - f_{ctm}$, where σ_1 and σ_2 were obtained from inverse analysis. There is an increase trend of σ_1 and σ_2 with f_{ctm}, but the corresponding regression coefficients are too low.

Fig. 15 represents the influence of the specimen's age and the percentage of binder replaced by Fa in the σ_1/f_{ctm} parameter. According to the results obtained, this parameter shows a tendency to decrease with the age. This indicates that the concrete age has a more pronounced effect on the material brittleness than on the material tensile strength, f_{ctm}.

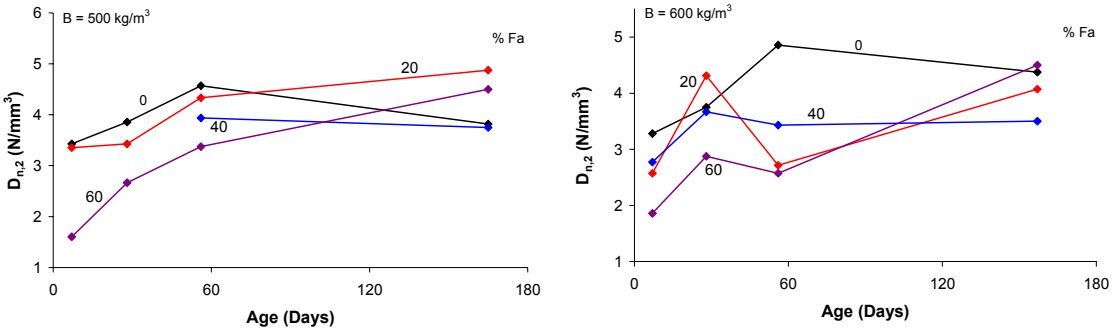

Fig. 13 - Influence of both the specimen's age and the percentage of binder replaced by *Fa* on $D_{n,2}$

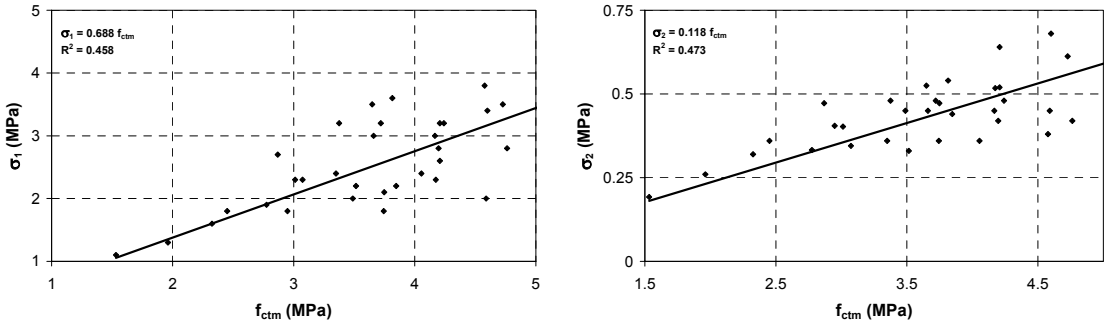

Fig. 14 - Relationships between σ_1 and σ_2 of the bilinear $\sigma - w$ diagram obtained from inverse analysis and f_{ctm} determined from experimental tests

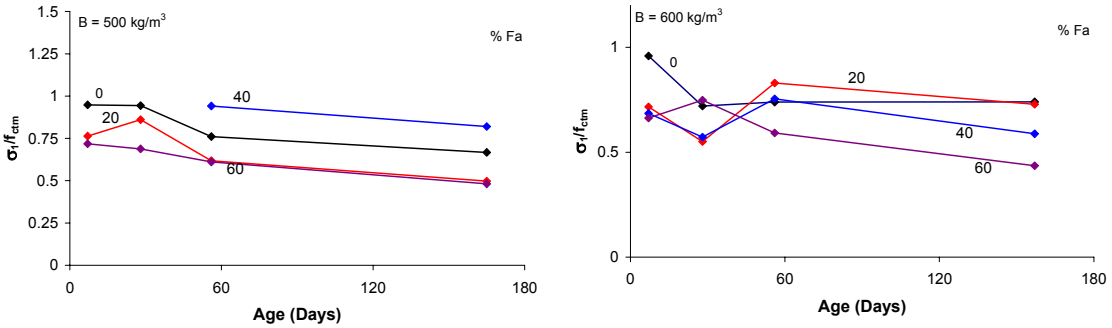

Fig. 15 - Influence of both the specimen's age and the percentage of binder replaced by *Fa* on σ_1 / f_{ctm}

5. CONCLUSIONS

To evaluate the fracture parameters of enhanced performance concrete, an inverse analysis was carried out using the force-deflection relationships obtained in three-point notched beam tests. In the FEMIX finite element package, where several types of finite elements and material constitutive models can be simultaneously used, a 2D line interface finite element was implemented to simulate crack propagation. The fracture mode I component of the 2D line interface finite element constitutive law was modelled with a bilinear stress-crack opening diagram ($\sigma - w$). The influence of both the concrete age when specimen was tested and the percentage of binder replaced by fly-ash (*Fa*) in the concrete fracture parameters was analysed. From the results obtained the following remarks can be pointed out:

- A bilinear $\sigma - w$ diagram is capable of simulating, with enough accuracy, the post-cracking behaviour of the enhanced performance concrete;
- The first stress point, σ_1, of the bilinear $\sigma - w$ diagram (stress at crack initiation) increased with the concrete age, having attained a maximum value for concrete specimens of 30 to 60 days old. After this age, the increase was marginal, and slight decreases were even reported in some series;
- The evolution of the second stress point, σ_2, of the bilinear $\sigma - w$ diagram was similar to σ_1, but the increase of σ_1 with the specimen's age was not so pronounced and was more lingering;

- In general, increasing the percentage of binder replaced by fly ash has decreased the values of σ_1 and σ_2;
- With the specimen's age the slope of the first branch of the bilinear $\sigma - w$ diagram, $D_{n,1}$, increased, having attained a maximum value in specimens with 30 to 60 days old. After 60 days $D_{n,1}$ remains stable or slightly decreases;
- In the majority of the series, the slope of the second branch of the bilinear $\sigma - w$ diagram, $D_{n,2}$, increased with the specimen's age, but this increase became less significant with the concrete age;
- With the concrete age, $D_{n,1}$ has decreased and $D_{n,2}$ has increased, mainly in the compositions with binder replaced by *Fa*;
- σ_1 and σ_2 have augmented with the increase of the uniaxial tensile strength, f_{ctm};
- Performing a linear regression analysis $\sigma_1 \cong 0.5 f_{ctm}$ and $\sigma_2 \cong 0.5 f_{ctm}$ were obtained, but the regression coefficients were too high;
- The parameter σ_1 / f_{ctm} has decreased with the specimen's age and its evolution was similar in the compositions with distinct percentage of binder replaced by fly ash.

ACKNOWLEDGEMENTS

The third author wishes to acknowledge the grant provided by PABERFIA research project supported by ADI.

REFERENCES

[1] - RILEM, Draft Recommendation, 50-FMC Committee Fracture Mechanics of Concrete, "Determination of the fracture energy of mortar and concrete by means of three-point bending tests on notched beams", Materials and Structures, V. 85, N. 85, pp. 285-290, (1985).

[2] - Gens, A., Carol, I., Alonso, E.E., "An interface element formulation for the analysis of soil-reinforcement interaction", Comp. and Geotechnics 7, pp. 133-151, (1988).

[3] - Janssen, J., "Mode-I fracture of plain concrete under monotonic and cyclic loading", Graduate thesis, Report TU Delft 25.2-90-2-05/TNO-IBBC BI-90-110, June (1990).

[4] - Melhorn, G., Kollegger, J., Keuser, M., Kolmar, W., "Nonlinear contact problems - a finite element approach implemented in ADINA", Comp. and Struct. 21(1/2), pp. 69-80, (1985).

[5] - Schellekens, J.C.J., "Interface elements in finite element analysis", TU-Delft report 25.2-90-5-17/TNO-IBBC report BI-90-165, October (1990).

[6] - Rots, J.G., "Computational modeling of concrete fracture", Dissertation, Delft University of Technology, (1988).

[7] - Richard, P., Cheyrezy, M.,"Les bétons de poudres réactives", Annales de l'ITBTP, 85-102, (1995) (*in French*)

[8] - Malhotra, V.M., Metha, P.K., "High-performance, high-volume fly ash concrete: materials, mixture proportioning, properties, construction practice, and case histories", Printed by Marquardt Printing Ltd., Ottawa, Canada, August (2002).

[9] - Azevedo, A.F.M.; Barros, J.A.O.; Sena-Cruz, J.M.; Gouveia, A.V., "Software no ensino e no projecto de estruturas (Software in structural engineering education and design)", III Portuguese-Mozambican Conference of Engineering, pp. 81-92, August (2003).

[10] - Zienkiewicz, O. C.; Taylor, R. L., The Finite Element Method, 4th Edition, McGraw-Hill, (1989.

[11] - Barros, J.A.O., "Behaviour of fibre reinforced concrete - experimental analysis and numerical simulation", PhD Thesis, Dep. of Civil Engineer of Oporto University, December (1995). (*in Portuguese*).

[12] - Vandewalle, L. *et al.*, "Test and design methods for steel fiber reinforced concrete. Design of steel fibre reinforced using σ-w method: principles and applications", Materials and Structures, Vol. 35, No 249, pp. 262-278, Jun. (2002).

[13] - Camões, A.F.L.L, "High performance concrete incorporating fly ash", PhD Thesis, University of Minho, July (2002) (*in Portuguese*).

[14] - CEB-FIP, "Model code 90 – design code", Thomas Telford, pp. 437 (1990).

[15] - Cunha, V.M.C.F., Ribeiro, A.F., Barros, J.A.O., Antunes, J.A.B., "Steel fibre reinforced concrete: recommendations and experimental and numerical research ", V Symposium EPUSP on Concrete Structures, Jun (2003) (*in Portuguese*).